Comparative Study of Direct-Contact and Air-Gap Membrane Distillation Processes

A. M. Alklaibi*,† and Noam Lior‡

Department of Mechanical Engineering, Jeddah College of Technology, P.O. Box 46716, Jeddah 21542, Kingdom of Saudi Arabia, and Department of Mechanical Engineering and Applied Mechanics, University of Pennsylvania, Philadelphia, Pennsylvania 19104-6315

Direct-contact and air-gap membrane distillation (DCMD and AGMD, respectively) processes have been modeled as a two-dimensional conjugate problem in which a simultaneous numerical solution of the momentum, energy, and diffusion equations of the feed and cold solutions have been carried out. The results were validated in comparison with available experimental results The two processes have been compared in terms of their sensitivity to the main parameters and the mass transfer resistances of the common domains. The results show, among other things, that the process thermal efficiency of AGMD is higher than that of DCMD by about 6% due to the presence of the air gap. The permeate flux of DCMD is higher than that of AGMD by about 2.3-fold and 4.8-fold for $T_{hi} = 80$ and 40 °C, respectively. Increase of the thermal conductivity of the membrane material (k_m) improves the DCMD process by mainly improving the process thermal efficiency and improves the AGMD process by mainly improving the permeate flux.

1. Introduction

Figure 1 shows a simple schematic of air-gap membrane distillation (AGMD), where an air gap is interposed between the membrane and the condensation surface, as well as the equivalent thermal resistances in each part. Elimination of that air gap together with the film condensate and the cooling plate results in the direct-contact membrane distillation (DCMD) process, where the membrane is in direct contact only with liquid phases, the water to be distilled (saline water in desalination applications) on one side and the liquid coolant used for condensation (fresh water in desalination) on the other. The main purpose of the air gap in AGMD is to reduce the heat loss represented by the parasitic (that does not contribute to the product flux) conduction heat flux from the membrane to the condensing surface; it was shown in a previous paper by the authors[1] that as the air gap width is increased from 1 to 5 mm, the heat transferred by conduction decreases 3.4-fold. The air gap, however, also increases the vapor mass transfer resistance between the cold surface of the membrane and the condensing surface and thus reduces the overall permeate flux for air gaps larger than a certain value (e.g., the permeate flux decreases 2.6-fold as the air gap thickness is increased from 1 to 5 mm[1]). DCMD, on the other hand, has less resistance to the mass transfer of water vapor, but it also has less resistance to the parasitic conductive heat transfer loss.

A fair amount of research has been performed on membrane distillation (MD) (cf. reviews in refs 2 and 3 and other work in refs 4−9), but a quantitative comparison between these two MD configurations is not available. This work models and compares the AGMD and DCMD processes, with emphasis on their permeate flux and thermal efficiency and their sensitivity to the hot solution inlet temperature (T_{hi}), cold solution inlet temperature (T_{ci}), feed solution concentration (w_{si}) and velocity (u_{hi}), the cold stream inlet velocity (u_{ci}), and the thermal conductivity of the membrane material (k_m).

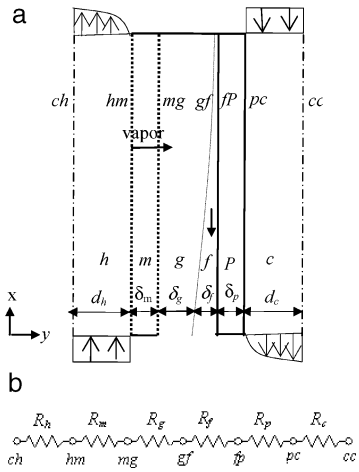

Figure 1. (a) AGMD model with domain and interface labels: (*h*) hot solution; (*m*) membrane; (*g*) airgap; (*f*) condensate film; (*p*) cooling plate; (*c*) cold fluid. The base-case model dimensions are $d_h = 2$ mm, $l_m = 0.2$ m, $\delta_m = 4 \times 10^{-4}$ m, $\delta_g = 3.5$ mm. (b) Thermal resistances in the model.

2. Theory

Figure 2 shows the DCMD model configuration (the system is symmetric along the flow direction, so only half of the cell is shown). The hot saline solution flows in the hot channel (h) and the cold coolant solution flows in the cold channel (c) in counterflow. Due to the difference in vapor pressure between the hot and cold side of the membrane that is caused by the difference in temperature, the saline water evaporates at the hot surface of the membrane (hm); the vapor penetrates through the membrane and condenses at the cold side of the membrane (mc) on the flowing fresh water coolant (c).

The hot saline solution flows between two parallel hydrophobic microporous membranes. The DCMD model is conjugate two-dimensional steady state, and the equations are in general similar to those we developed for the AGMD model.[1]

* To whom all correspondence should be addressed. Phone: +96657482736. E-mail: klaibi@seas.upenn.edu.
† Jeddah College of Technology.
‡ University of Pennsylvania.

10.1021/ie051094u CCC: $37.00
Published on Web 12/09/2006

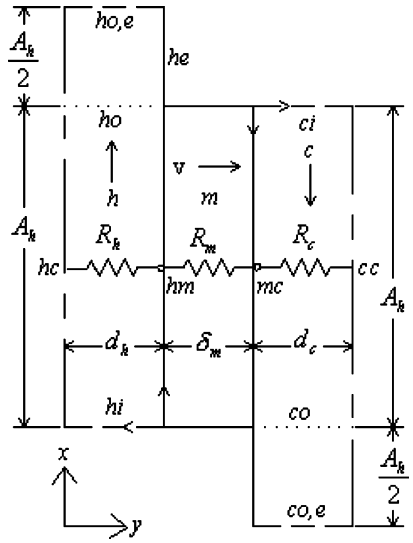

Figure 2. DCMD model configuration.

This is a significant advancement over existing models,[4−9] which are one-dimensional nonconjugate. The transport of the momentum, energy, and species of the hot solution are described by the continuity, momentum, energy, and species conservation equations,[10] which are normalized by using the dimensionless variables

$$\bar{x}_h = \frac{x_h}{d_h}, \quad \bar{y}_h = \frac{y_h}{d_h}, \quad \bar{u}_h = \frac{u_h}{u_{hi}}, \quad \bar{v}_h = \frac{v_h}{u_{hi}}, \quad \bar{P}_h = \frac{P_h}{\rho_S u_{hi}^2},$$
$$\bar{T}_h = \frac{T_h - T_{ci}}{T_{hi} - T_{ci}}, \quad \bar{w}_s = \frac{w_s}{w_{si}} \quad (1)$$

where d_h is the distance between the membrane surface and the center of the hot solution channel, u_{hi} is the inlet velocity of the hot solution, T_{hi} and T_{ci} are the inlet temperatures of the hot and cold solutions, respectively, and w_{si} is the mass fraction of salt (here NaCl) in water at the entrance of the channel.

The fluids are Newtonian, and viscous dissipation is ignored, as it is of importance only at high velocities. An order-of-magnitude analysis of the viscous term has shown it to be about 4−5 orders of magnitude smaller than the dominant terms in the energy equation.

While the solution properties (c_p, k, μ, ρ) change with temperature and concentration, they were assumed in our model to be constant, at the midrange value for each run, because of the following:[1] (1) The temperature variations are relatively small, with the thermal conductivity variation over that range being only 1%, that of specific heat being 0.1%, and that of density being 0.6%. The variation of the viscosity is about 10%, but the influence of this variation on the sought results is negligible because experimental work has shown that the effect of the viscosity on the flux is less than that of the concentration of salt, which has been shown to have a very small effect on the flux anyway. (2) The physical properties are affected little by the concentration of NaCl: for a 3-fold increase in the concentration, from 20 000 to 60 000 ppm, the thermal conductivity and specific heat are almost unaffected; density increased by 2.2%, and viscosity, by 4.5%. (3) The diffusion coefficient of vapor through air varies by at most 4.5% within that studied range of temperatures and pressures.

Considering the general modeling error, we believe therefore that the additional effort of computing temperature- and concentration-dependent properties would have made the computation longer and more difficult yet yielded little improvement.

The dimensionless equations are

$$\frac{\partial \bar{u}_h}{\partial \bar{x}_h} + \frac{\partial \bar{v}_h}{\partial \bar{y}_h} = 0 \quad (2)$$

$$\bar{u}_h \frac{\partial \bar{u}_h}{\partial \bar{x}_h} + \bar{v}_h \frac{\partial \bar{u}_h}{\partial \bar{x}_h} = -\frac{\partial \bar{P}_h}{\partial \bar{x}_h} + \frac{1}{Re_h}\left(\frac{\partial^2 \bar{u}_h}{\partial \bar{x}_h^2} + \frac{\partial^2 \bar{u}_h}{\partial \bar{y}_h^2}\right) \quad (3)$$

$$\bar{u}_h \frac{\partial \bar{v}_h}{\partial \bar{x}_h} + \bar{v}_h \frac{\partial \bar{v}_h}{\partial \bar{y}_h} = -\frac{\partial \bar{P}_h}{\partial \bar{y}_h} + \frac{1}{Re_h}\left(\frac{\partial^2 \bar{v}_h}{\partial \bar{x}^2_h} + \frac{\partial^2 \bar{v}_h}{\partial \bar{y}_h^2}\right) \quad (4)$$

$$\left(\bar{u}_h \frac{\partial \bar{T}_h}{\partial \bar{x}_h} + \bar{v}_h \frac{\partial \bar{T}_h}{\partial \bar{y}_h}\right) = \frac{1}{Re_h Pr_h}\left(\frac{\partial^2 \bar{T}_h}{\partial \bar{x}_h^2} + \frac{\partial^2 \bar{T}_h}{\partial \bar{y}_h^2}\right) \quad (5)$$

$$\left(\bar{u}_h \frac{\partial \bar{w}_s}{\partial \bar{x}_h} + \bar{v}_h \frac{\partial \bar{w}_s}{\partial \bar{y}_h}\right) = \frac{1}{Re_h S_c}\left(\frac{\partial^2 \bar{w}_s}{\partial \bar{x}_h^2} + \frac{\partial^2 \bar{w}_s}{\partial \bar{y}_h^2}\right) \quad (6)$$

where the Reynolds, Prandtl, and Schmidt numbers of the hot solution are, respectively,

$$Re_h = \frac{\rho_S u_{hi} d_h}{\mu_S}, \quad Pr_h = \frac{\mu_s c_{ps}}{k_s}, \quad Sc_h = \frac{\nu_S}{D_S} \quad (7)$$

The continuity, momentum, and energy equations in the cooling solution are normalized by using the dimensionless variables

$$\bar{x}_c = \frac{x_c}{d_h}, \quad \bar{y}_c = \frac{y_c}{d_h}, \quad \bar{u}_c = \frac{u_c}{u_{ci}}, \quad \bar{v}_c = \frac{v_c}{u_{ci}}, \quad \bar{P}_c = \frac{P_c}{\rho_S u_{ci}^2},$$
$$\bar{T}_c = \frac{T_c - T_{ci}}{T_{hi} - T_{ci}} \quad (8)$$

and the equations are

$$\frac{\partial \bar{u}_c}{\partial \bar{x}_c} + \frac{\partial \bar{v}_c}{\partial \bar{y}_c} = 0 \quad (9)$$

$$\bar{u}_c \frac{\partial \bar{u}_c}{\partial \bar{x}_c} + \bar{v}_c \frac{\partial \bar{u}_c}{\partial \bar{y}_c} = -\frac{\partial \bar{P}_c}{\partial \bar{x}_c} + \frac{1}{Re_c}\left(\frac{\partial^2 \bar{u}_c}{\partial \bar{x}_c^2} + \frac{\partial^2 \bar{u}_c}{\partial \bar{y}_c^2}\right) \quad (10)$$

$$\bar{u}_c \frac{\partial \bar{v}_c}{\partial \bar{x}_c} + \bar{v}_c \frac{\partial \bar{v}_c}{\partial \bar{y}_c} = -\frac{\partial \bar{P}_c}{\partial \bar{y}_c} + \frac{1}{Re_c}\left(\frac{\partial^2 \bar{v}_c}{\partial \bar{x}_c^2} + \frac{\partial^2 \bar{v}_c}{\partial \bar{y}_c^2}\right) \quad (11)$$

$$\left(\bar{u}_c \frac{\partial \bar{T}_c}{\partial \bar{x}_c} + \bar{v}_c \frac{\partial \bar{T}_c}{\partial \bar{y}_c}\right) = \frac{1}{Re_c Pr_c}\left(\frac{\partial^2 \bar{T}_c}{\partial \bar{x}_c^2} + \frac{\partial^2 \bar{T}_c}{\partial \bar{y}_c^2}\right) \quad (12)$$

where the Reynolds and Prandtl numbers of the cold solution are defined, respectively, as

$$Re_c = \frac{\rho_S u_{ci} d_c}{\mu_S}, \quad Pr_c = \frac{\mu_s c_{ps}}{k_s} \quad (13)$$

Because the cold channel contains pure water, the species conservation equation is not needed here.

Boundary Conditions. The boundary conditions at the inlet of the channels (hi, ci), outlet of the channels (ho, co), center of the channels (hc, cc), hot surface of the membrane (hm), and cold surface of the membrane (mc) read as follows.

Inlet Interfaces (hi, ci).

$$\bar{u}_h = 1, \quad \bar{v}_h = 0, \quad \bar{T}_h = 1, \quad \bar{w}_s = 1 \tag{14}$$

$$\bar{u}_c = 1, \quad \bar{v}_c = 0, \quad \bar{T}_c = 0 \tag{15}$$

Center of the Channel Interfaces (hc, cc).

$$\frac{\partial \bar{u}_h}{\partial \bar{y}_h} = 0, \quad \bar{v}_h = 0, \quad \frac{\partial \bar{T}_h}{\partial \bar{y}_h} = 0, \quad \frac{\partial \bar{w}_s}{\partial \bar{y}_h} = 0 \tag{16}$$

$$\frac{\partial \bar{u}_c}{\partial \bar{y}_c} = 0, \quad \bar{v}_c = 0, \quad \frac{\partial \bar{T}_c}{\partial \bar{y}_c} = 0 \tag{17}$$

Outlet of Channels Interfaces (hoe, coe). As commonly done in computational fluid mechanics, it is assumed that the static pressure along an outflow (or inflow) boundary surface is constant relative to a known reference pressure and that the boundary-parallel component of the static pressure gradient is zero (this condition is much more useful and frequently more realistic than the sometimes-used condition that the boundary-normal component of the static pressure gradient is zero).

$$\bar{P}_h = 0 \tag{18}$$

$$\bar{p}_c = 0 \tag{19}$$

Outlet of the Channel Interfaces (ho, co). The convective term is much (about 8−9 orders of magnitude[1]) larger than the conductive term in the energy equation and the diffusive term in the diffusion equation at the hot solution channel exit, and hence, the heat and mass flux equations can be approximated as follows

$$(u_{hi}\rho_S C_{pS}\bar{u}_h\bar{T}_h + k_S\Delta\bar{T}_h)\cdot\vec{n} \approx u_{hi}\rho_S C_{pS}\bar{u}_h\bar{T}_h\cdot\vec{n} \tag{20}$$

$$(u_{hi}\bar{u}_h\bar{w}_s + D_S\Delta\bar{w}_s)\cdot\vec{n} \approx u_{hi}\bar{u}_h w_s\cdot\vec{n} \tag{21}$$

$$(u_{ci}\rho_S C_{pS}\bar{u}_c\bar{T}_c + k_S\Delta\bar{T}_c)\cdot\vec{n} \approx u_{hi}\rho_S C_{pS}\bar{u}_c\bar{T}_c\cdot\vec{n} \tag{22}$$

where $\vec{n}$ is a unit vector normal to the outlet interface.

Membrane Hot Surface Interface (hm).

$$\bar{u}_h = 0 \tag{23}$$

$$\bar{v}_h = \frac{J_v}{u_{hi}\rho_s} \tag{24}$$

$$-k_s\frac{d\bar{T}_h}{d\bar{y}_h} = \frac{d_h(Q_C + J_v h_{fg})}{T_{hi} - T_{ci}} \tag{25}$$

$$\frac{D_S}{d_h}\frac{\partial \bar{w}_s}{\partial \bar{y}_h} = \frac{J_v}{w_{si}\rho_S} \tag{26}$$

Cold Side of the Membrane (mc)

$$\bar{u}_c = 0 \tag{27}$$

$$\bar{v}_c = \frac{J_v}{u_{ci}\rho_S} \tag{28}$$

$$-k_S\frac{d\bar{T}_c}{d\bar{y}_c} = \frac{d_h(Q_C + J_v h_{fg})}{T_{hi} - T_{ci}} \tag{29}$$

3. Process Parameters

The parameters to be evaluated in this work include the averaged permeate flux and the process thermal efficiency.

The averaged permeate flux is obtained by

$$J = \frac{1}{l_m}\int_0^{l_m} J_v(x)\,dx \tag{30}$$

where l_m is the membrane length, and the local permeate flux is calculated from

$$J_v(x) = K\Delta P_v \tag{31}$$

where the vapor pressures (P_v) were calculated using the Antoine equation

$$\ln P_v = A_1 - \frac{A_2}{T_{hm} - A3} \tag{32}$$

where $A_1 = 16.2620$, $A_2 = 3799.89$, and $A_3 = -226.35$, P_v is in Pascal, and T_{hm} is in degrees Celsius. The validity of this equation was checked by comparison to the steam tables and was found to be accurate to better than 0.4% within the 40−80 °C temperature range studied in this paper. K is the permeability of the membrane, defined (when air is present in the membrane) as

$$K = \frac{\epsilon D_{v/a} M_v P_T}{\chi\delta_m P_{a,avg} R_u T_{avg,m}} \tag{33}$$

where ϵ (porosity) and χ (tortuosity) are membrane geometry parameters, $D_{v/a}$ is the diffusion coefficient of the vapor through the air, $P_{a,avg}$ is the average partial pressure of the air, P_T is the total (air + vapor) pressure, and

$$T_{avg,m} = \frac{T_{hm} + T_{mg}}{2} \tag{34}$$

The effect of the presence of the salt in the solution on the vapor pressure at the hot surface of the membrane has been accounted for by using the empirical correlation for the boiling point elevation.[11]

The process thermal efficiency can be defined as

$$\eta_t = \frac{\tilde{Q}_L}{\tilde{Q}_T} \tag{35}$$

where $\tilde{Q}_L$ is the heat transfer due to production of the distillate and the total heat transfer across the membrane ($\tilde{Q}_T$) is

$$\tilde{Q}_T = \tilde{Q}_L + \tilde{Q}_C \tag{36}$$

where the x-averaged conductive heat transfer is

$$\tilde{Q}_C = \frac{1}{l_m}\int_0^{l_m} Q_C(x)\,dx \tag{37}$$

with the local conductive heat flux calculated as

$$Q_C = \frac{T_{hm} - T_{mc}}{R_m} \tag{38}$$

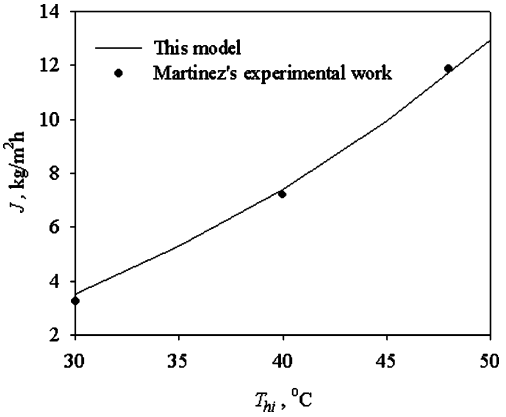

Figure 3. Effect of the temperature on the permeate flux, as in this study, in comparison with the DCMD experiments of ref 4. $T_{ci} = 14$ °C, $u_{hi} = 0.31$ m s^{-1}, $d_h = 1$ mm, $l_m = 5.5$ cm, $\delta_m = 1.25 \times 10^{-4}$ m, $u_{ci} = 0.31$ m s^{-1}, $\epsilon = 0.75$, $\chi = 1.7$, and $k_m = 0.22$ W m^{-1} K^{-1}.

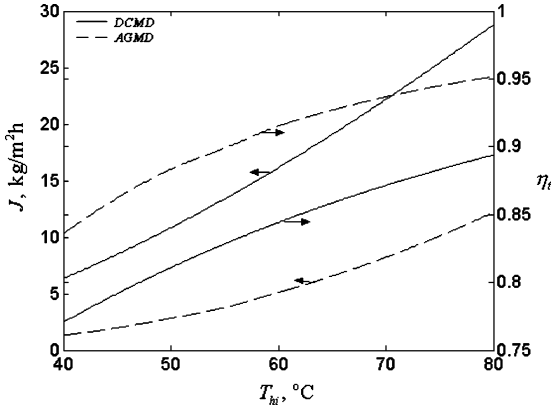

Figure 4. Effect of the inlet temperature of the hot solution (T_{hi}) on the permeate flux (J) and the process thermal efficiency (η_t) for AGMD and DCMD. $T_{ci} = 20$ °C, $u_{hi} = 0.1$ m s^{-1} ($Re_h = 464$), $w_{si} = 0.025$, $d_h = 0.002$ m, $l_m = 0.2$ m, $\delta_m = 4 \times 10^{-4}$ m, $\chi = 1.5$, $k_m = 0.2$ W m^{-1} K^{-1}, $\epsilon = 0.78$, $\delta_g = 2$ mm, $k_p = 60$ W m^{-1} K^{-1}, $\delta_p = 1.5 \times 10^{-3}$ m, $u_{ci} = 0.1$ m s^{-1} ($Re_c = 193$), and $d_c = 0.002$ m.

where

$$R_m = \frac{\delta_m}{k_{me}} \tag{39}$$

with

$$k_{me} = \epsilon k_a + (1 - \epsilon)k_m \tag{40}$$

The temperatures at the hot side of the membrane, T_{hm}, and cold side of the membrane, T_{mc}, needed to evaluate these parameters are found from the solution of the transport equations explained above.

4. Method of Solution, Grid Independence, and Validation

The Femlab finite element program[12] was used for the solution. A grid-dependence analysis of the method of solution was performed. The number of elements is chosen to be 13 258 because further refinement of the mesh to 29 926 elements produced just a 0.03% difference in J.

The computed results for DCMD were validated by comparison with Martinez and Florido-Diaz's DCMD experimental ones[5] and were found to be in very good agreement, within about 5%, as shown in Figure 3. The membrane pore tortuosity used in the comparison was computed from the quantity $\epsilon/\chi/\delta = 3300$ m^{-1}, given in the reference, and was found to be 1.7.

Our AGMD model was successfully validated by comparison with the experimental results of Banat,[8] as reported in ref 1.

5. Results and Discussion

The sensitivity of the permeate flux (J) and of the process thermal efficiency (η_t) to the main parameters is analyzed. These include the temperature (T_{hi}), concentration (w_{si}) and velocity (u_{hi}) at the hot saline feed solution inlet, the temperature (T_{ci}) and velocity (u_{ci}) at the cold fluid inlet, and the thermal conductivity of the membrane material (k_m).

5.1. Effect of the Hot Solution Inlet Temperature. Figure 4 shows the effect of the inlet temperature of the hot solution (T_{hi}) on the permeate flux (J) and the process thermal efficiency (η_t) for AGMD and DCMD. The J and η_t values of both processes increase as T_{hi} increases. The η_t value of AGMD increases by about 11.6%, and that of DCMD, by 12% as T_{hi} is increased from 40 to 80 °C. For the same range, J of AGMD increases by more than 9-fold and the value for DCMD increases by more than 4-fold. Figure 4 also shows that η_t of DCMD is lower than that of AGMD: by 6.5% at $T_{hi} = 40$ °C and by 5.8% at $T_{hi} = 80$ °C. DCMD has a lower η_t because of the higher conductive heat transfer ($\tilde{Q}_C$), which results from the elimination of the air gap resistance (R_g).

The thermal efficiency increases with T_{hi} because of the resulting increase of the permeate flux with T_{hi}, and that increases the heat transfer due to production of the distillate ($\tilde{Q}_L$). As can be seen from the definition of η_t (eqs 35 and 36), a higher rate increase of $\tilde{Q}_L$ than the conductive heat flow $\tilde{Q}_C$ will increase η_t.

Although DCMD has a slightly lower η_t than AGMD, it produces higher permeate fluxes in the entire tested range of T_{hi}, as shown in Figure 4. J in DCMD is higher than that of AGMD by 4.8-fold at $T_{hi} = 40$ °C and by 2.36-fold at $T_{hi} = 80$ °C, resulting mainly from the increase in the temperature difference between the two membrane surfaces.

The higher fluxes result in a reduction of the membrane area required for the process and thus a corresponding reduction of the capital cost of the process. At $T_{hi} = 80$ °C, the area required for DCMD is about 57% less than that required by AGMD for the same flux. The slight increase of the process thermal efficiency of AGMD is thus well-compensated by the significantly higher flux of DCMD.

5.2. Effect of Inlet Temperature of the Cold Solution. The effect of the cold solution inlet temperature (T_{ci}) on the permeate flux (J) and thermal process efficiency (η_t) is shown in Figure 5. Lowering T_{ci} increases J but decreases η_t for both processes. For AGMD, decreasing T_{ci} from 45 to 5 °C increases J by more than 2-fold, and for DCMD, J increases by 1.8-fold over the same range. For DCMD, the rate of the increase becomes slower as T_{ci} decreases. For example, when T_{ci} decreases from 45 to 25 °C, J increases by 1.53-fold as opposed to 1.18-fold when T_{ci} decreases from 25 to 5 °C. This is because of the decrease of the contribution of the mass transfer resistance of the cold fluid to the total mass transfer resistance as T_{ci} decreases. The analysis of mass transfer resistances of the AGMD and DCMD is explained in detail in ref 13.

The value of η_t for DCMD is more sensitive to T_{ci} than *that* of AGMD. Decreasing T_{ci} from 45 to 5 °C decreases the η_t of AGMD by about only 2% and by 12% for DCMD. T_{ci} has more influence on the η_t of DCMD than that of AGMD, in part because of the slower rate of the increase in J of DCMD at low temperature and the increase of the conductive heat transfer ($\tilde{Q}_C$)

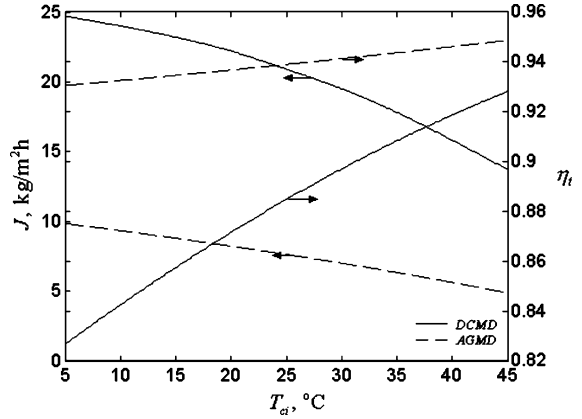

Figure 5. Effect of the inlet temperature of the cold solution (T_{ci}) on the permeate flux (J) and the process thermal efficiency (η_t) for AGMD and DCMD. T_{hi} = 70 °C, u_{hi} = 0.1 m s^{-1} (Re_h = 464), w_{si} = 0.025, d_h = 0.002 m, l_m = 0.2 m, δ_m = 4 × 10^{-4} m, χ = 1.5, k_m = 0.2 W m^{-1} K^{-1}, ϵ = 0.78, δ_g = 2 mm, k_p = 60 W m^{-1} K^{-1}, δ_p = 1.5 × 10^{-3} m, u_{ci} = 0.1 m s^{-1} (Re_c = 193), and d_c = 0.002 m.

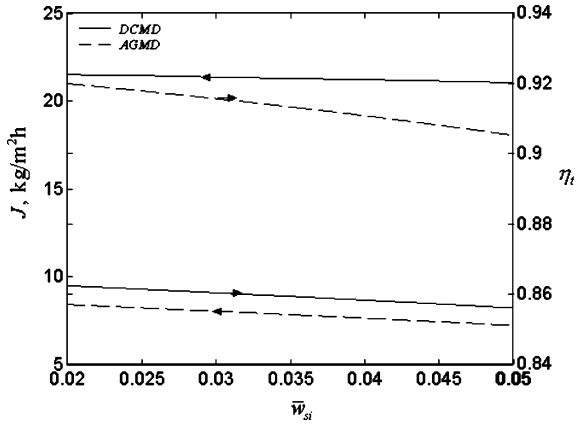

Figure 6. Effect of the hot solution inlet concentration (w_{si}) on the permeate flux (J) and the process thermal efficiency (η_t), T_{hi} = 70 °C, T_{ci} = 20 °C, u_{hi} = 0.1 m s^{-1} (Re_h = 464), d_h = 0.002 m, l_m = 0.2 m, δ_m = 4 × 10^{-4} m, χ = 1.5, k_m = 0.2 W m^{-1} K^{-1}, ϵ = 0.78, δ_g = 2 mm, k_p = 60 W m^{-1} K^{-1}, δ_p = 1.5 × 10^{-3} m, u_{ci} = 0.1 m s^{-1} (Re_c = 193), and d_c = 0.002 m.

to larger extent in DCMD as T_{ci} decreases which resulted from the absence of the air gap resistance in DCMD.

5.3. Effect of the Inlet Concentration of the Hot Solution. The inlet concentration of the feed solution (w_{si}) has a moderate effect on the process. AGMD is more affected by the inlet concentration of the feed solution than DCMD, as shown in Figure 6. As w_{si} is increased from 20 000 to 50 000 ppm, J is reduced by only 3% for DCMD and by 16% for AGMD. AGMD is more sensitive to the concentration of the solution because of the larger proportion of the reduction of the vapor pressure at the hot surface of the membrane (hm) on the driving force of the process. In other words, because the driving force ($P_{hm} - P_{cm}$) of DCMD is larger than the driving force ($P_{hm} - P_{gm}$) of the AGMD, thereby, the effect of the reduction of P_{hm} has more impact on the flux in AGMD.

As shown in Figure 6, the process thermal efficiency of DCMD is practically unaffected by the inlet concentration of the feed solution and that of AGMD is reduced by 2% as w_{si} is increased from 20 000 to 50 000 ppm.

5.4. Effect of the Inlet Velocity of the Hot Solution. Figure 7 shows the effect of the velocity of the hot stream (u_{hi}) on the permeate flux (J) and the process thermal efficiency (η_t). For both processes, J increases as u_{hi} increases but with different proportions. J increases by 11% for AGMD and twice as much as that for DCMD. η_t on the other hand is almost unaffected

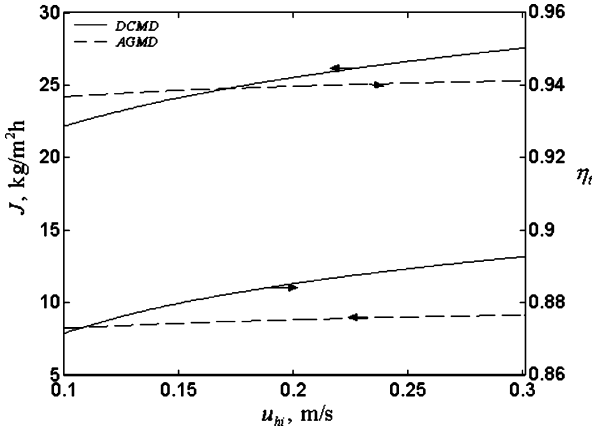

Figure 7. Effect of the inlet velocity of the hot stream (u_{hi}) on the permeate flux (J) and the process thermal efficiency (η_t). T_{hi} = 70 °C, T_{ci} = 20 °C, w_{si} = 0.025, d_h = 0.002 m, l_m = 0.2 m, δ_m = 4 × 10^{-4} m, χ = 1.5, k_m = 0.2 W m^{-1} K^{-1}, ϵ = 0.78, δ_g = 2 mm, k_p = 60 W m^{-1} K^{-1}, δ_p = 1.5 × 10^{-3} m, u_{ci} = 0.1 m s^{-1} (Re_c = 193), and d_c = 0.002 m.

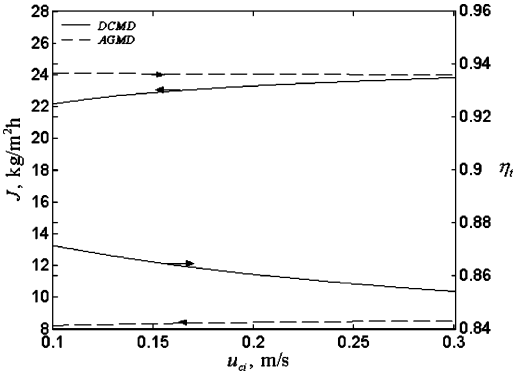

Figure 8. Effect of the inlet velocity of the cold stream (u_{ci}) on the permeate flux (J) and the process thermal efficiency (η_t). T_{hi} = 70 °C, T_{ci} = 20 °C, u_{hi} = 0.1 m s^{-1} (Re_h = 464), w_{si} = 0.025, d_h = 0.002 m, l_m = 0.2 m, δ_m = 4 × 10^{-4} m, χ = 1.5, k_m = 0.2 W m^{-1} K^{-1}, ϵ = 0.78, δ_g = 2 mm, k_p = 60 W m^{-1} K^{-1}, δ_p = 1.5 × 10^{-3} m, and d_c = 0.002 m.

for both processes. For the same range of u_{hi} from 0.1 to 0.3 m s^{-1}, the η_t of AGMD increases by less than 1% and by 2% for DCMD. J in DCMD is more sensitive to u_{hi} because of the larger portion of the mass transfer resistance of the hot stream (R_{Mh}) of DCMD to the total mass transfer resistance (R_{MT}).[13]

5.5. Effect of the Inlet Velocity of the Cold Solution. Figure 8 shows the effect of the inlet velocity of the cold stream (u_{ci}) on the permeate flux (J) and the process thermal efficiency (η_t). Increasing u_{ci} from 0.1 to 0.3 m s^{-1} has a slight impact on J; it increases the J of DCMD by 7% and the J of AGMD by only 4%. This small impact resulted from the small ratio of the mass transfer resistance of the cold solution (R_{Mc}) to the total mass transfer resistance (R_{MT}). On the other hand, it increases the conductive heat transfer ($\tilde{Q}_C$) as shown in Figure 9. The small improvement of J combined with the larger increase in $\tilde{Q}_C$ causes η_t to decrease as u_{ci} increases. This is more noticeable for DCMD as the increase of $\tilde{Q}_C$ is larger.

It noteworthy that the effect of the inlet velocity of the hot fluid is stronger than that of the cold fluid, as described in more detail in ref 13. This is because the mass transfer resistance of the hot solution is a larger fraction of the total mass transfer resistance than the mass transfer resistance of the cold liquid. Since increasing the solution velocity decreases the mass transfer resistance, the effect is larger for the hot solution than the cold one.

5.6. Effect of the Thermal Conductivity of the Membrane Material. Figure 10 shows the effect of the thermal conductivity

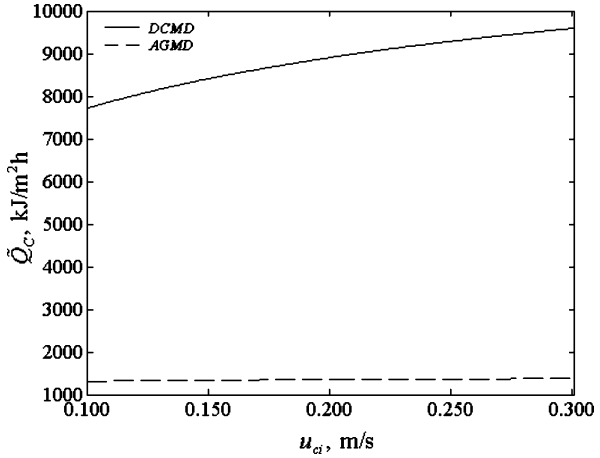

Figure 9. Effect of the inlet velocity of the cold stream (u_{ci}) on the conductive heat transfer ($\tilde{Q}_C$). T_{hi} = 70 °C, T_{ci} = 20 °C, u_{hi} = 0.1 m s^{-1} (Re_h = 464), w_{si} = 0.025, d_h = 0.002 m, l_m = 0.2 m, $\delta_m = 4 \times 10^{-4}$ m, χ = 1.5, k_m = 0.2 W m^{-1} K^{-1}, ϵ = 0.78, δ_g = 2 mm, k_p = 60 W m^{-1} K^{-1}, $\delta_p = 1.5 \times 10^{-4}$ m, and d_c = 0.002 m.

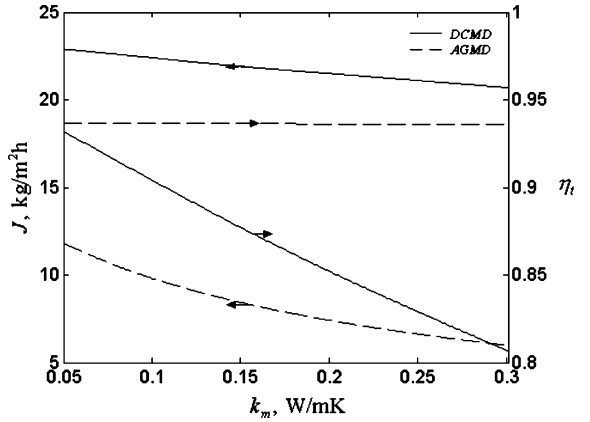

Figure 10. Effect of the thermal conductivity of the membrane material (k_m) on the permeate flux (J) and the process thermal efficiency (η_t). T_{hi} = 70 °C, T_{ci} = 20 °C, u_{hi} = 0.1 m s^{-1} (Re_h = 464), w_{si} = 0.025, d_h = 0.002 m, l_m = 0.2 m, $\delta_m = 4 \times 10^{-4}$ m, χ = 1.5, ϵ = 0.78, δ_g = 2 mm, k_p = 60 W m^{-1} K^{-1}, $\delta_p = 1.5 \times 10^{-3}$ m, u_{ci} = 0.1 m s^{-1} (Re_c = 193), and d_c = 0.002 m.

of the membrane material (k_m) on the permeate flux (J) and the process thermal efficiency (η_t). The J value of DCMD is less sensitive to the thermal conductivity of the membrane material (k_m) than that of AGMD. For DCMD, J increases 1.1-fold as the thermal conductivity is lowered from 0.3 to 0.05 W m^{-1} K^{-1}. For AGMD, J increases 1.96-fold. That is because, in the AGMD configuration, the temperature at the membrane cold side (mg) is determined by balancing the sensible heat transfer of both sides of the membrane which is a function of the membrane thermal resistance (R_m, eq 39), and any variation of R_m affects the driving force of AGMD ($P_{hm} - P_{mg}$). On the other hand, in DCMD, the membrane cold side temperature (T_{mc}) is mainly determined by the thermal resistance of the cold stream (R_c), and thus, the driving force ($P_{hm} - P_{mc}$) of DCMD is affected less by R_m. The figure also shows that the η_t values of DCMD and AGMD are improved by reducing the thermal conductivity of the membrane material, but this improvement is more noticeable for DCMD; opposite to the effect of k_m on J. As k_m is reduced from 0.3 to 0.05 W m^{-1} K^{-1}, η_t of DCMD improves by 12.5% and η_t of AGMD improves by about 6%. This is because the total thermal resistance of AGMD is dominated by the thermal resistance of the air gap (R_g), and the thermal resistance of the membrane (R_m) is in series with R_g, as shown in Figure 1b, and thus has only a slight impact on

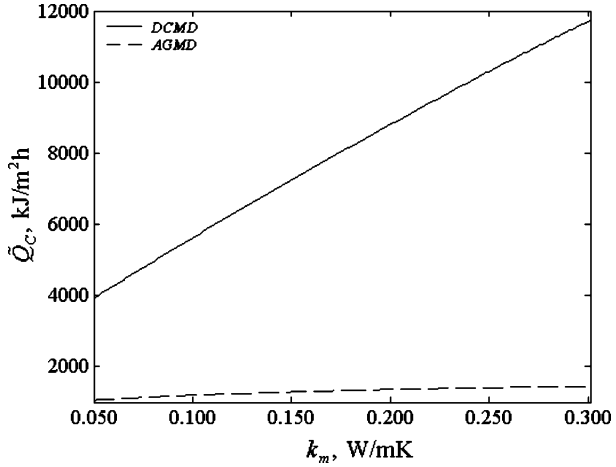

Figure 11. Effect of the thermal conductivity of the membrane material (k_m) on the conductive heat transfer ($\tilde{Q}_C$). T_{hi} = 70 °C, T_{ci} = 20 °C, u_{hi} = 0.1 m s^{-1} (Re_h = 464), w_{si} = 0.025, d_h = 0.002 m, l_m = 0.2 m, $\delta_m = 4 \times 10^{-4}$ m, χ = 1.5, ϵ = 0.78, δ_g = 2 mm, k_p = 60 W m^{-1} K^{-1}, $\delta_p = 1.5 \times 10^{-3}$ m, u_{ci} = 0.1 m s^{-1} (Re_c = 193), and d_c = 0.002 m.

the conductive heat transfer ($\tilde{Q}_C$) as shown in Figure 11. On the other hand, the air gap is absent in DCMD, and thus, R_m becomes the controlling thermal resistance; thereby, the membrane thermal conductivity will have a much more significant impact on $\tilde{Q}_C$, as shown in Figure 11. So, for DCMD, η_t is more significantly improved by using membrane materials with low thermal conductivity.

To summarize, decreasing k_m improves the DCMD process mainly by improving the process thermal efficiency and improves the AGMD process by mainly improving the permeate flux.•

6. Conclusions

- The processes thermal efficiency of AGMD is higher than that of DCMD by about 6% due to the presence of the air gap.
- The permeate flux in DCMD is higher than that in AGMD by about 2.3-fold at T_{hi} = 80 °C and becomes even higher for low inlet feedwater hot temperatures: at T_{hi} = 40 °C, J_{DCMD}/J_{AGMD} = 4.8.
- Decreasing the inlet temperature of the cold steam (T_{ci}) lowers the process thermal efficiency of DCMD to a larger extent than that of AGMD and increases the flux to a lesser extent. One can conclude that for a more efficient DCMD process, the inlet temperature of the cold solution should not be very low (<10 °C), because that will increase the conductive heat transfer more significantly than increasing the permeate flux, thus lowering the process thermal efficiency.
- Increasing the inlet velocity of the hot solution (u_{hi}) has more positive impact on improving the DCMD process (i.e., increasing the permeate flux and the process thermal efficiency) than it does on improving AGMD.
- The inlet velocity of the cold solution (u_{ci}) has little effect on both the permeate flux and the process thermal efficiency of AGMD, but increasing it lowers the process thermal efficiency and increases the permeate flux of DCMD somewhat.
- The thermal conductivity of the membrane material (k_m) improves the DCMD process by mainly improving the process thermal efficiency and improves the AGMD process by mainly improving the permeate flux.

Nomenclature

A_1,A_2,A_3 = see eq 32
c_s = mole fraction of NaCl

C_p = specific heat, kJ kg^{-1} K^{-1}
D_s = diffusion coefficient of the NaCl, m^2 s^{-1}
d_h = half-width of the flow channel, m
J = length-averaged permeate flux at the hot side of the membrane, kg m^{-2} h^{-1}
J_v = local permeate flux at the hot side of membrane, in vapor phase, kg m^{-2}s^{-1}
K = permeability of the membrane, s^{-1}
k = thermal conductivity, W m^{-1} K^{-1}
l_m = membrane length, m
m = membrane
P = pressure, Pa
Q = heat transferred, kJ m^{-2} h^{-1}
$\bar{Q}$ = average heat transfer, kJ m^{-2} h^{-1}
R = thermal resistance, W m^{-2} K^{-1}
Re_h = Reynolds number of the hot solution channel, eq 7
Re_c = Reynolds number of the cold solution channel, eq 13
T = temperature, °C
$\bar{T}_c = (T_c - T_{ci})/(T_{hi} - T_{ci})$
$\bar{T}_h = (T_h - T_{ci})/(T_{hi} - T_{ci})$
u_c = the velocity in x_c direction, m s^{-1}
$\bar{u}_c = u_c/u_{ci}$
u_{ci} = the velocity at the inlet of the cold channel, m s^{-1}
u_h = the velocity in x_h direction, m s^{-1}
$\bar{u}_h = u_h/u_{hi}$
u_{hi} = the velocity at the inlet of the hot channel, m s^{-1}
v = y component of feed solution velocity, m s^{-1}
v_c = the velocity in y_c direction, m s^{-1}
v_h = the velocity in y_h direction, m s^{-1}
x_c = coordinate along the solution flow in the cold channel, m
$\bar{x}_c = x_c/d_h$
x_h = coordinate along the solution flow in the hot channel, m
$\bar{x}_h = x_h/d_h$
y_c = coordinate normal to the solution flow in the cold channel, m
$\bar{y}_c = y_c/d_h$
y_h = coordinate normal to the solution flow in the hot channel, m
$\bar{y}_h = y_h/d_h$
w_s = mass fraction of NaCl
$\bar{w}_s = w_s/w_{si}$
w_{si} = inlet value of the mass fraction of NaCl

Greeks

b = volume coefficient of expansion, K^{-1}
ΔP = water vapor pressure difference between the membrane, Pa
ΔT_g = temperature difference between the air gap hot and cold sides, °C
d = thickness or width, m
e = porosity
η_t = process thermal efficiency
m = dynamic viscosity, kg m^{-1} s^{-1}
r = density, kg m^{-3}
c = tortuosity

Subscripts

a = air
atm = atmosphere
c = cold solution
cc = center line of cold channel
ci = inlet of the cold channel
ch = center line of the hot channel
co = outlet of the cold channel
pc = cooling plate/cold channel interface
e = effective
f = condensate film
fp = condensate film/cooling plate interface
g = vapor/air gap
gf = air gap/condensate film interface
mg = membrane/air gap interface
h = hot channel
hi = inlet of the hot channel
hm = hot liquid/membrane interface
ho = outlet of the hot channel
l = liquid water
m = membrane
p = cooling plate
S = solution
T = total
v = vapor

Literature Cited

(1) Alklaibi, A. M.; Lior, N. Transport analysis of air-gap membrane distillation. *J. Membr. Sci.* **2005**, *255*, 239.
(2) Lawson, K.; Lloyd, D. Review membrane distillation. *J. Membr. Sci.* **1997**, *24*, 1.
(3) Alklaibi, A. M.; Lior, N. Membrane-distillation desalination: status and potential. *Desalination* **2004**, *171*, 111.
(4) Lawson, K. W.; Lloyd, D. R. Membrane distillation. II. Direct contact MD. *J. Membr. Sci.* **1996**, *120*, 123.
(5) Martinez, L.; Florido-Diaz, F. J. Theoretical and experimental studies on desalination using membrane distillation. *Desalination* **2001**, *139*, 373.
(6) Phattaranawik, J.; Jiraratananon, R. Direct contact membrane distillation: effect of mass transfer on heat transfer. *J. Membr. Sci.* **2001**, *188*, 137.
(7) Jonsson, A. S.; Wimmerstedt, R.; Harrysson, A. C. Membrane distillation-A theoretical study of evaporation through microporous membranes. *Desalination* **1985**, *56*, 237.
(8) Banat, F. Membrane distillation for desalination and removal of volatile organic compounds from water. Ph.D. Dissertation, McGill University, Montreal, Canada, 1994.
(9) Liu, G.; Zhu, C.; Cheung, S.; Leung, C. W. Theoretical and experimental studies on air gap membrane distillation. *Heat Mass Transfer* **1998**, *34*, 329.
(10) Bird, R. B.; Steward, W. E.; Lightfoot, E. N. *Transport Phenomena*; Wiley: New York, 1960.
(11) Fabuss, B. M.; Korosi, A. Boiling point elevations of seawater and its concentrates. *J. Chem. Eng. Data* **1966**, *11*, 606.
(12) *FEMLAB*, release 2.3; COMSOL, Inc.: 8 NE Executive Park, Suite 310, Burlington, MA 01803, 2002; www.Femlab.com.
(13) Alklaibi, A. M.; Lior, N. Heat and mass transfer resistance analysis of membrane distillation. *J. Membr. Sci.* **2005**, *282*, 362.

Received for review September 30, 2005
Revised manuscript received September 25, 2006
Accepted October 17, 2006

IE051094U